Construction of a spanning tree for high-order edge elements

Eduardo de Los Santos, Ana Maria Alonso Rodríguez, Francesca Rapetti

Received: Added at production | Revised: Added at production | Accepted: Added at production

DOI: xxx/xxxx

ARTICLE TYPE

Construction of a spanning tree for high-order edge elements

Eduardo De Los Santos[1] | Ana Maria Alonso Rodríguez[1] | Francesca Rapetti[2]

[1]Dip. di Matematica, Univ. di Trento, Povo, Trento, Italy
[2]Dept. de Mathématiques., Univ. Côte d'Azur, Nice, France

Correspondence
*Eduardo De Los Santos Email: eduardo.santos.nunez@gmail.com

Present Address
Dip. di Matematica, Univ. di Trento, via Sommarive 14, I-38123 Povo, Trento

Summary

The well-known tree-cotree gauging method for low-order edge finite elements is extended to high-order approximations within the first family of Nédélec finite element spaces. The key point in this method is the identification of degrees of freedom for edge and nodal finite element spaces such that the matrix of the gradient operator is the transposed of the all-node incidence matrix of a directed graph. This is straightforward for low-order finite elements and it can be proved that it is still possible in the high-order case using either moments or weights as degrees of freedom. In the case of weights, the geometrical realization of the graph associated with the gradient operator is very natural. We recall in details the definition of weights and present an algorithm for the construction of a spanning tree of this graph. The starting point of the algorithm is a spanning tree of the graph given by vertices and edges of the mesh (the so-called global spanning tree, that is the one used in the low-order case). This global step, interpreted in the high-order sense, is enriched locally, with a loop over the elements of the mesh, with arcs corresponding to edge, face and volume degrees of freedom required in the high-order case.

KEYWORDS:
High-order edge elements, tree-cotree gauge, small simplices' graph, incidence matrix.

1 | INTRODUCTION

The aim of this work is to present the construction of a spanning tree of the graph associated with the degrees of freedom (dofs) of high-order nodal and edge finite elements to extend the well-known tree-cotree gauging method. The idea of the tree-cotree gauge is to identify a set of dofs for edge finite elements that spans the kernel of the curl operator. If the domain is simply connected, these dofs are identified on a spanning tree of the graph whose nodes (arcs) are the dofs of nodal (edge) elements, respectively. Using the weights[1,2,3] as dofs for high-order edge and nodal finite elements, the graph can be thought on a particular refinement (associated with the *principal lattice*) of the elements of the initial mesh. The small tetrahedra generated by this (virtual) refinement are affine contractions of those of the initial mesh and are called small elements. They are not constructed actually (and in this sense they are virtual), however they allow for a geometrical localization of the previously referred graph and thus for a suitable visualization of the dofs for high-order nodal and edge elements for any polynomial degree. The construction of a spanning tree of this graph is not more involved than the construction of a spanning tree of the well-known vertex-edge graph of the original mesh. Indeed, the visualization o the new selected arcs, namely those that do not result from the splitting of edges of the mesh, is the same in all the faces and at the interior of all the tetrahedra of the mesh. If the domain is not simply connected, the kernel of the curl operator is bigger than the image of the gradient operator. The spanning tree has to be enriched of one edge (called, the fastener) for each generator of the first homology group, thus resulting on a "belted" spanning tree[4,5].

Whitney edge elements[6] are widely recognized as a useful tool for computational electromagnetism[5]. They offer a simple construction of polynomial differential forms on simplicial complexes[7,8]. Their associated dofs have a very clear physical meaning (circulation of the approximated

[0]**Abbreviations:** Spanning tree for high-order edge elements

field on the edges of the element)[6]. Because they model the curl kernel well, the matrix associated with the curl-curl operator is singular, and this singularity is related to the graph whose *geometrical realization* is the finite element mesh. Specifically when the domain is simply connected, a tree-cotree decomposition of the arcs of this graph is used to classify dofs into dependent and independent ones for the curl operator[9]. In fact, a vector potential with fixed values of its independent dofs (identified by means of the tree) is unique[10,11]. This was successfully applied in a three-dimensional magnetostatic problem[12] and also in a nonlinear eddy current problem[13].

In the development of high-order extensions of Whitney edge elements, the classical approach[14,15,16] introduces moments to define the needed dofs. Such a construction includes dofs associated with faces and tetrahedra that can not be interpreted as field circulations along edges and consequently it does not allow for an immediate geometrical realization of its associated graph. The approach proposed in[1,17,18] generalizes to higher orders the methodology of Whitney: if one finds a way to represent a manifold of dimension k by a k-chain (i.e., formal sum of mesh simplices of dimension k) then by duality one knows how to represent a field by a finite weighted sum of basis fields (the Whitney forms).

In this work, we follow this approach that yields new dofs for high-order approximations, the so-called *weights*[3,19,20]. In the case of nodal elements, they are the classical functionals that associate with a function its values at the *small vertices*, that are the nodes of the principal lattices of the mesh elements. In the case of edge elements, they are functionals that associate with a field its circulations along the *small edges*, that are the edges of the *small tetrahedra*[2,18]. These weights are relevant, since they pop up naturally when we generalize Whitney construction to the high-order case. Note that, each small edge can be localized either (i) on an edge of the mesh, or (ii) at the interior of a face of the mesh or (iii) at the interior of an element of the mesh. The small edges for high-order extensions of Whitney 1-forms are always linking adjacent points of the principal lattice of the same order. They have the same orientation and are parallel to edges of the mesh. When dofs are weights, the matrix representative of the gradient is an incidence matrix (between small edges and small vertices) for any polynomial degree[21]. On the other hand, the duality property between unisolvent dofs (circulations on small edges) and generators of the finite element space is lost in the high-order case if all the edges of the small tetrahedra are considered. Duality is recovered by choosing an appropriate subset[22] of the small edges. The resulting graph, with the principal lattices of the mesh elements as nodes and this subset of small edges as arcs, is an oriented connected graph. Let us consider the canonical basis of the nodal and edge finite element spaces for the weights supported on the nodes and arcs of this graph respectively. In this context, we are interested in the matrix that represents the gradient as a linear operator between finite dimensional spaces. This means, the matrix that computes the circulations along the small edges of a field that is the gradient of a nodal finite element function, knowing the values of this function at the nodes of the principal lattices of the mesh elements. It is easy to see that this matrix is the transpose of the all-node incidence matrix of the graph. In the simply connected case, the gradients of the nodal finite elements fill-in the kernel of the curl operator acting on edge finite element functions. Then the selection of a spanning tree of this graph is a useful tool for the identification of high-order potentials[23] or for the tree-cotree gauge within high-order approximations. In this contribution we propose an efficient algorithm for the construction of a spanning tree of this graph.

The outline of this work is as follows. In Section 2 we introduce the fundamental notion of small simplices. In Section 3 we explain how to use this notion to define basis and dofs for high-order Whitney finite elements, and we introduce the high-order graph induced by the supports of these dofs. We then relate this graph with the matrix that represents the gradient operator on the canonical bases. Finally in Section 4 we present the algorithm for the construction of a spanning tree of the high-order graph and some considerations on its particularities.

2 | SMALL SIMPLICES

Let $\mathcal{T} = (V, E, F, T)$ be a tetrahedral mesh of the polyhedral domain Ω of $\mathbb{R}^3$, where V is the set of vertices, E is the set of edges, F is the set of faces, and T is the set of tetrahedra of $\mathcal{T}$. Let $\Delta_d(\mathcal{T})$ denote the set of d-simplices of the mesh, for $d \in \{0,1,2,3\}$, thus $\Delta_0(\mathcal{T}) = V$, $\Delta_1(\mathcal{T}) = E$, $\Delta_2(\mathcal{T}) = F$, and $\Delta_3(\mathcal{T}) = T$. Let us fix an orientation on each edge, face, and tetrahedron of $\mathcal{T}$. This can be done by choosing a total ordering of the vertices in $V = \{\mathbf{v}_i\}_{i=1}^{N_V}$ and by associating with each d-simplex of the mesh, $S \in \Delta_d(\mathcal{T})$, an increasing function $m_S : \{0,1,\dots,d\} \to \{1,\dots,N_V\}$. The oriented d-simplex S is hence given by $S = [\mathbf{v}_{m_S(0)}, \dots, \mathbf{v}_{m_S(d)}]$.

For $S \in \Delta_d(\mathcal{T})$, we denote by $\Delta_\ell(S)$ the set of ℓ-simplices contained in S, for $\ell \in \{0,\dots,d\}$. For each $\Sigma \in \Delta_\ell(S)$ with $\ell \in \{0,\dots,d-1\}$, if $S = [\mathbf{v}_{m_S(0)}, \dots, \mathbf{v}_{m_S(d)}]$ and $\Sigma = [\mathbf{v}_{m_\Sigma(0)}, \dots, \mathbf{v}_{m_\Sigma(\ell)}]$, then there exists a unique increasing map $m_\Sigma^S : \{0,\dots,\ell\} \to \{0,\dots,d\}$ such that, for each $i \in \{0,\dots,\ell\}$, $m_\Sigma(i) = m_S(m_\Sigma^S(i))$.

For $r, d \in \mathbb{N}$, let us set

$$\mathcal{I}(d+1, r) := \{\boldsymbol{\eta} = (\eta_0, \dots, \eta_d) \in \mathbb{N}^{d+1} \,:\, |\boldsymbol{\eta}| = r\},$$

being $|\boldsymbol{\eta}| := \sum_{i=0}^{d} \eta_i$. The cardinality of $\mathcal{I}(d+1, r)$ is equal to $\binom{r+d}{d} = \frac{(r+d)!}{r!d!}$.

For a point $\mathbf{x}$ in a d-simplex $S \in \Delta_d(\mathcal{T})$ (with $d \in \{1,2,3\}$), we denote by $\boldsymbol{\lambda}_S(\mathbf{x}) = (\lambda^S_{m_S(0)}(\mathbf{x}), \dots, \lambda^S_{m_S(d)}(\mathbf{x}))$ the vector of its barycentric coordinates with respect to the vertices $\{\mathbf{v}_{m_S(0)}, \dots, \mathbf{v}_{m_S(d)}\}$ of S. Each function $\lambda^S_{m_S(\ell)} : S \to \mathbb{R}$ satisfies the property $\lambda^S_{m_S(\ell)}(\mathbf{v}_{m_S(j)}) = \delta_{j,\ell}$,

with $\ell, j \in \{0,\dots,d\}$. The functions $\lambda^S_{m_S(\ell)}$ are positive at the interior of S, and non negative on S. The barycentric coordinates also satisfy the properties of representation of points and partition of unity, namely

$$\mathbf{x} = \sum_{j=0}^{d} \lambda^S_{m_S(j)}(\mathbf{x})\mathbf{v}_{m_S(j)} \text{ and } \sum_{j=0}^{d} \lambda^S_{m_S(j)}(\mathbf{x}) = 1\,.$$

Let $t \in T$, for each $i \in \{1,\dots,n_V\}$ we denote $\lambda_i : \overline{\Omega} \to \mathbb{R}$

$$\lambda_i : \mathbf{x} \mapsto \lambda_i(\mathbf{x}) = \begin{cases} \lambda^t_{m_t(\ell)}(\mathbf{x}) & \text{if } \mathbf{x} \in t \text{ and } i = m_t(\ell) \text{ with } \ell \in \{0,\dots,3\} \\ 0 & \text{otherwise.} \end{cases}$$

The set of real valued polynomials defined on S of degree less than or equal to r is denoted by $\mathcal{P}_r(S)$ and the subspace of $\mathcal{P}_r(S)$ of homogeneous polynomials of degree r is denoted by $\tilde{\mathcal{P}}_r(S)$. We have $\dim\mathcal{P}_r(S) = \binom{r+d}{d}$ and $\dim\tilde{\mathcal{P}}_r(S) = \binom{r+d-1}{d}$. When S is reduced to a single point, then $\mathcal{P}_r(S) = \mathbb{R}$ for all $r \geq 0$. For any S, if $r < 0$, then $\mathcal{P}_r(S) = \{0\}$. It is known that the barycentric coordinate functions $\lambda^S_{m_S(i)}$ constitute a basis for $\mathcal{P}_1(S)$. Given $S \in \Delta_d(\mathcal{T})$ and $\boldsymbol{\alpha} \in \mathcal{I}(d+1, r)$, we define the continuous function

$$\boldsymbol{\lambda}^{\boldsymbol{\alpha}}_S : \mathbf{x} \mapsto \boldsymbol{\lambda}^{\boldsymbol{\alpha}}_S(\mathbf{x}) = \Pi^d_{j=0}\left[\lambda^S_{m_S(j)}(\mathbf{x})\right]^{\alpha_j}.$$

It holds that $\mathcal{P}_r(S) = \text{Span}_{\boldsymbol{\alpha}\in\mathcal{I}(d+1,r)}\{\boldsymbol{\lambda}^{\boldsymbol{\alpha}}_S\}$.

Definition 1 (Principal lattice of order $r+1$)**.** Given $S = [m_S(0),\dots,m_S(d)]$ and an integer $r \geq 0$, the principal lattice of order $r+1$ in the d-simplex S is the set of points

$$L_{r+1}(S) = \left\{\mathbf{x} \in S \,:\, \lambda^S_{m_S(j)}(\mathbf{x}) \in \left\{0, \frac{1}{r+1}, \frac{2}{r+1}, \dots, \frac{r}{r+1}, 1\right\},\ 0 \leq j \leq d\right\}.$$

Equivalently,

$$L_{r+1}(S) = \left\{\mathbf{x} \in S \,:\, \mathbf{x} = \frac{1}{|\boldsymbol{\beta}|}\sum_{j=0}^{d} \beta_j \mathbf{v}_{m_S(j)},\ \ \forall\, \boldsymbol{\beta} \in \mathcal{I}(d+1, r+1)\right\}.$$

In what follows, to give a general definition (in the sense of the ambient dimension q) of the *small ℓ-simplices* (with $0 \leq \ell \leq q$), we consider a mesh $\widetilde{\mathcal{T}}$ of a q-dimensional domain $\widetilde{\Omega}$, where $S \in \Delta_q(\widetilde{\mathcal{T}})$ is a triangle (resp. tetrahedron) when $q = 2$ (resp. $q = 3$).

Definition 2 (Small ℓ-simplex)**.** Let $S \in \Delta_q(\widetilde{\mathcal{T}})$ and $\boldsymbol{\alpha} \in \mathcal{I}(q+1, r)$, for an integer $r \geq 0$. The small q-simplex $\{\boldsymbol{\alpha}, S\}$ is the q-simplex with barycenter

$$\frac{1}{r+1}\sum_{j=0}^{q}\left[\left(\frac{1}{q+1} + \alpha_i\right)\mathbf{v}_{m_S(j)}\right]$$

and $1/(r+1)$-homothetic to S. For any $\Sigma \in \Delta_\ell(S)$, the small ℓ-simplex $\{\boldsymbol{\alpha}, \Sigma\}$ is the ℓ-simplex which is parallel, equally oriented to Σ and belongs to the small q-simplex $\{\boldsymbol{\alpha}, S\}$.

It is worth noting that the small q-simplices do not pave the q-simplex S. In other words, depending on r, geometric shapes not homothetic to S, such as octahedra or reversed tetrahedra (resp. reversed triangles) for $q = 3$ (resp. $q = 2$), appear together with the small q-simplices in each $S \in \Delta_q(\widetilde{\mathcal{T}})$ to completely pave S (as detailed in Table 1).

Number and type of shapes associated with $L_{r+1}(S)$			
in a tetrahedron S	$\binom{r+3}{3}$ small tetrahedra	$\binom{r+2}{3}$ octahedra	$\binom{r+1}{3}$ reversed tetrahedra
in a triangle S	$\binom{r+2}{2}$ small triangles	$\binom{r+1}{2}$ reversed triangles	
in a segment S	$\binom{r+1}{1}$ small edges		

TABLE 1 Number of small ℓ-simplices, for $\ell > 0$, and other shapes in a ℓ-simplex S as a function of the polynomial degree $r+1$, with $r \geq 0$.

In Figure 1 is presented a triangle $f = [n_0, n_1, n_2]$ together with its principal lattice $L_{r+1}(f)$ for $r = 2$. In grey we have the corresponding family of small simplices. In Figure 2 we have the small simplices associated with the principal lattice $L_3(t)$ in a tetrahedron $t = [n_0, n_1, n_2, n_3]$. The resulting decomposition of t includes 10 small tetrahedra, and also 4 octahedra and 1 reversed tetrahedron. On each face of the boundary of t we can see 6 small faces and 3 reversed triangles. Note that each edge of t is decomposed in 3 small edges.

The small simplices are of key importance in the generalization of Whitney finite elements to higher order. Indeed, they allow to make a list of the generators of any polynomial degree of the finite element spaces and constitute the support of new dofs, the weights, for the representation

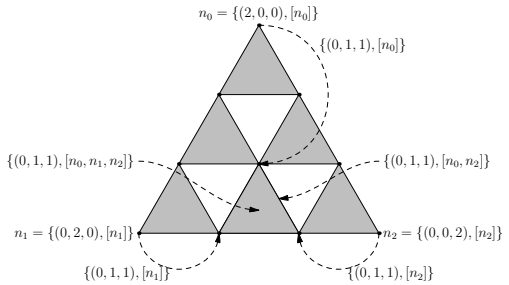

FIGURE 1 Principal lattice $L_3(f)$ in the face $f = [n_0, n_1, n_2]$, with the visualization of all the small simplices. The label of the small simplex $\{(0,1,1),[n_0,n_1,n_2]\}$ and of some of its sub-simplices are indicated for illustration.

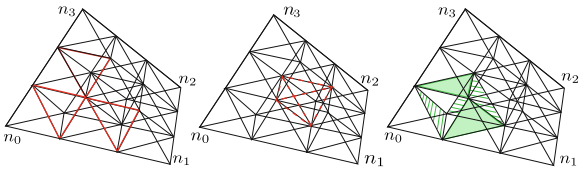

FIGURE 2 (Taken from reference [25]). Principal lattice $L_3(t)$ in the tetrahedron $t = [n_0, n_1, n_2, n_3]$, with the visualization of all the small simplices. Each face of the boundary of t is decomposed in 6 small faces and 3 reversed triangles (highlighted on the left with red solid lines). The decomposition of t includes 10 small tetrahedra, 1 reversed tetrahedron (highlighted at the center with red dashed lines) and 4 octahedra (one is highlighted on the right in green).

of fields in these spaces (together with a direct geometrical visualization of the tree-cotree structure that we discuss in the last part of the present work).

3 | HIGH-ORDER WHITNEY EDGE ELEMENTS AND THE HIGH-ORDER GRAPH

For a more compact presentation, we rely on the notation of the finite element exterior calculus. It is well known (see [24,20]) that the proxy fields of the space of trimmed polynomial differential forms (usually denoted by $\mathcal{P}^-_{r+1}\Lambda^k(\mathcal{T})$) are the finite element space of Lagrange of degree $r+1 \geq 1$ if $k = 0$, the first family of Nédélec finite elements of order $r+1$ conforming in $H(\mathrm{curl};\Omega)$ if $k = 1$, the first family of Nédélec finite elements of order $r+1$ conforming in $H(\mathrm{div};\Omega)$ if $k = 2$, and discontinuous elements of degree $\leq r$ if $k = 3$. Let d be the exterior derivative for differential k-forms for $k < d$.

Definition 3 (Whitney k-forms). In a tetrahedron t, Whitney k-forms associated with $S \in \Delta_k(t)$ are the fields

$$w_S = \begin{cases} \lambda_{m_S(0)}, & \text{with } k = 0,\ S = [n_{m_S(0)}], \\ \sum_{j=0}^{k} (-1)^j \lambda_{m_S(j)} \mathrm{d}\, w_{S-[n_{m_S(j)}]}, & \text{with } k > 0,\ S = [n_{m_S(0)}, \ldots, n_{m_S(k)}]. \end{cases}$$

In particular, for $k = 1$ the exterior derivative d corresponds to the gradient operator and Definition 3 yields

$$w_S = \lambda_{m_S(0)} \,\mathrm{grad}\, \lambda_{m_S(1)} - \lambda_{m_S(1)} \,\mathrm{grad}\, \lambda_{m_S(0)}.$$

Whitney k-forms of higher degree in each tetrahedron t can be associated with the principal lattice in t as recalled in the next Definition.

Definition 4 (High-order Whitney k-forms). In a tetrahedron t, Whitney k-forms of higher polynomial degree are the fields

$$w_s = \boldsymbol{\lambda}_t^{\boldsymbol{\alpha}} w_S,$$

for all the small k-simplices $s := \{\boldsymbol{\alpha}, S\}$, with $\boldsymbol{\alpha} \in \mathcal{I}(4,r)$ for $r > 0$, and $S \in \Delta_k(t)$, being w_S the Whitney k-form associated with S. The space of high-order Whitney k-forms in t is

$$\mathcal{P}^-_{r+1}\Lambda^k(t) = \mathsf{Span}\ \{w_s\ :\ s = \{\boldsymbol{\alpha}, S\}, \boldsymbol{\alpha} \in \mathcal{I}(4,r), S \in \Delta_k(t)\}\,.$$

Fields in $\mathcal{P}^-_{r+1}\Lambda^k(t)$ are defined as products between a field in $\mathcal{P}^-_1\Lambda^k(t)$ and the continuous function $\boldsymbol{\lambda}^{\boldsymbol{\alpha}}_t$, with $\boldsymbol{\alpha} \in \mathcal{I}(4,r)$. Therefore, fields in $\mathcal{P}^-_{r+1}\Lambda^k(t)$ enjoy the same conformity properties as those in $\mathcal{P}^-_1\Lambda^k(t)$ [3].

Definition 5 (Weights on small k-simplices). For a polynomial k-form $u \in \mathcal{P}^-_{r+1}\Lambda^k(t)$, with $0 \leq k \leq 3$ and $r \geq 0$, the weights are the real numbers

$$\int_{\{\boldsymbol{\alpha},S\}} u, \tag{1}$$

for all the small k-simplices $\{\boldsymbol{\alpha}, S\}$, with $\boldsymbol{\alpha} \in \mathcal{I}(4,r)$ and $S \in \Delta_k(t)$.

The weights of a high-order Whitney k-form $u \in \mathcal{P}^-_{r+1}\Lambda^k(t)$ along all the small k-simplices $\{\boldsymbol{\alpha}, S\}$ of a mesh $\mathcal{T}$ are *unisolvent* [25, Proposition 3.14], namely if $u \in \mathcal{P}^-_{r+1}\Lambda^k(t)$ is such that $\int_{\{\boldsymbol{\alpha},S\}} u = 0$ for all the small k-simplices $s = \{\boldsymbol{\alpha}, S\}$, then $u = 0$. The small k-simplices can thus support the dofs for fields $u \in \mathcal{P}^-_{r+1}\Lambda^k(t)$. Since the result on unisolvence holds true also by replacing t with $\Sigma \in \Delta_\ell(t)$ (for $k \leq \ell < 3$), then the respective trace of u over any $\Sigma \in \Delta_\ell(t)$ (trace that lives in $\mathcal{P}^-_{r+1}\Lambda^k(\Sigma)$) is uniquely determined by the weights localized on small k-simplices in Σ. We thus can use the weights on the small k-simplices $\{\boldsymbol{\alpha}, S\}$ as dofs for the fields in the finite element space $\mathcal{P}^-_{r+1}\Lambda^k(\mathcal{T})$, being aware that their number is greater than the dimension of the space.

The weights given in Definition 5 have a meaning as cochains and this relates directly the matrix describing the exterior derivative with the matrix of the boundary operator. The key point is the Stokes theorem $\int_C \mathrm{d}u = \int_{\partial C} u$, where u is a $(k-1)$-form and C a k-chain. More precisely, if $u \in \mathcal{P}^-_{r+1}\Lambda^{k-1}(\mathcal{T})$ then $\mathrm{d}u \in \mathcal{P}^-_{r+1}\Lambda^k(\mathcal{T})$ and

$$\int_{\{\boldsymbol{\alpha},S\}} \mathrm{d}u = \int_{\partial\{\boldsymbol{\alpha},S\}} u = \sum_{\{\boldsymbol{\beta},\Sigma\}} \mathtt{B}_{\{\boldsymbol{\alpha},S\},\{\boldsymbol{\beta},\Sigma\}} \int_{\{\boldsymbol{\beta},\Sigma\}} u, \tag{2}$$

being $\mathtt{B}$ the *boundary matrix* with as many rows as small k-simplices, and as many columns as small $(k-1)$-simplices. The small k-simplex $\{\boldsymbol{\alpha}, S\}$ inherits the orientation of the k-simplex S, so the coefficient $\mathtt{B}_{\{\boldsymbol{\alpha},S\},\{\boldsymbol{\beta},\Sigma\}}$ is equal to the coefficient $\mathtt{B}_{S,\Sigma}$ of the boundary of the simplex S if $\boldsymbol{\beta} = \boldsymbol{\alpha}$ and zero otherwise. Therefore, $\mathtt{B}_{S,\Sigma}$ is 1 or -1 depending of whether the orientation of Σ matches or not with the orientation induced by that of the k-simplex S on its $(k-1)$-face Σ, and $\mathtt{B}_{S,\Sigma}$ is zero when Σ is not part of the boundary of S. This fact is straightforward if $\dim(\Sigma) > 0$, but also when $\dim(\Sigma) = 0$ [21]. For $k = 1$, note that the matrix $\mathtt{B}_{\{\boldsymbol{\alpha},S\},\{\boldsymbol{\beta},\Sigma\}}$ is an incidence matrix between small edges and small vertices; moreover, it is an all-node incidence matrix of a (non connected) graph, whose geometrical realization is shown on the right of Figure 3.

Remark: For $k = 1$, in order to have $\mathtt{B}$ an incidence matrix between small edges and small vertices, some points in the principal lattice have different labels. The point $\frac{1}{|\boldsymbol{\eta}|}\sum_{j=0}^{3}\left[\left[\frac{1}{4}+\eta_j\right]\mathbf{v}_{m_t(j)}\right] \in L_3(t)$, with $\boldsymbol{\eta} = (2,0,1,0)$ has a label as the small vertex $\{(2,0,0,0),[n_2]\}$ (the brown point in the fragmented visualization) and also as the small vertex $\{(1,0,1,0),[n_0]\}$ (the black point in the fragmented visualization). However, the 0-forms associated with the different labels are the same. Indeed, $\{(2,0,0,0),[n_2]\}$ corresponds with the 0-form $\lambda^2_{m_t(0)}w_{n_2} = \lambda^2_{n_0}\lambda_{n_2}$ and $\{(1,0,1,0),[n_0]\}$ with the 0-form $\lambda_{m_t(0)}\lambda_{m_t(2)}w_{n_0} = \lambda_{n_0}\lambda_{n_2}\lambda_{n_0} = \lambda^2_{n_0}\lambda_{n_2}$, and we can see that "both" 0-forms are actually the same.

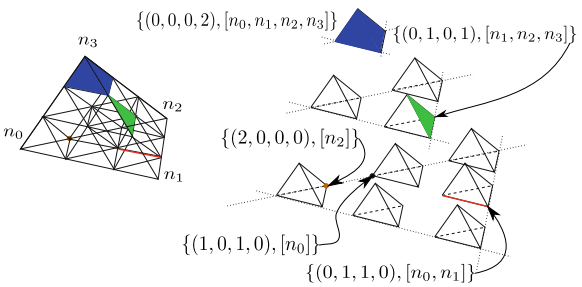

FIGURE 3 (Taken from reference [21]). Visualization (on the left) of all the small simplices associated with the principal lattice $L_3(t)$ in the tetrahedron $t = [n_0, n_1, n_2, n_3]$. The same set of small simplices in a fragmented visualization (on the right), a small tetrahedron in blue, a small face in green, a small edge in red and small vertex in brown and also in black (note the different labels for the same point in the principal lattice $L_3(t)$).

We say that a set of unisolvent degrees of freedom for high-order Whitney finite elements is minimal if its cardinality is equal to the dimension of the finite element space. In order to use a set of minimal unisolvent degrees of freedom for high-order Whitney edge finite elements, we have to disregard some small edges. In fact, it can be proved [22] that to be unisolvent it is enough to consider on each face small edges parallel to two of the three edges of the face, and on each tetrahedron small edges parallel to three of the six edges of the tetrahedra. Proceeding in this way, the corresponding set of weights is unisolvent and minimal.

We use the term *active* to indicate all the small k-simplices such that $\boldsymbol{\lambda}_t^{\boldsymbol{\alpha}} w_S$ belongs to a basis of $\mathcal{P}^-_{r+1}\Lambda^k(\mathcal{T})$. The dimension of the space $\mathcal{P}^-_{r+1}\Lambda^k(\mathcal{T})$ coincides with the number of *active small k-simplices* in the mesh $\mathcal{T}$ [23]. We recall the following result [26, Proposition 6.4]:

Proposition 1 (A basis of $\mathcal{P}^-_{r+1}\Lambda^k(t)$). The set $\left\{\boldsymbol{\lambda}_t^{\boldsymbol{\alpha}} w_S \,:\, \boldsymbol{\alpha} \in \mathcal{I}(4,r),\, S \in \Delta_k(t) \text{ and } \alpha_j = 0 \text{ if } j < m_S^t(0)\right\}$ is a basis of $\mathcal{P}^-_{r+1}\Lambda^k(t)$.

A possible rule for selecting the active small vertices $\{\boldsymbol{\alpha}, [n_i]\}$ and set of active small edges $\{\boldsymbol{\alpha}, [n_{m_e(0)}, n_{m_e(1)}]\}$, that induces minimal and unisolvent weights, is the same given in Proposition 1 to select a basis of $\mathcal{P}^-_{r+1}\Lambda^k(t)$.

We denote by d_L and d_N the dimension of $\mathcal{P}^-_{r+1}\Lambda^0(\mathcal{T})$ and $\mathcal{P}^-_{r+1}\Lambda^1(\mathcal{T})$, respectively. We consider the graph $\mathcal{G}_{ho}$ with nodes the set $\{\mathbf{q}_\ell\}_{\ell=1}^{d_L}$ of active small vertices (the points of the principal lattices of the mesh elements) and arcs the set $\{\mathbf{e}_m\}_{m=1}^{d_N}$ of active small edges. Let $\{\phi_{h,i}\}_{i=1}^{d_L}$ and $\{\boldsymbol{\omega}_{h,j}\}_{j=1}^{d_N}$ be the canonical bases of the nodal and edge finite element spaces for the weights supported on the nodes and arcs of this graph, respectively. This means that $\phi_{h,i}(\mathbf{q}_\ell) = \delta_{i,\ell}$ and $\int_{\mathbf{e}_m} \boldsymbol{\omega}_{h,j} = \delta_{j,m}$, where $\delta_{\cdot,\cdot}$ is the Kronecker delta. For each active small edge $\mathbf{e}_m$, we denote by $\mathbf{q}_{m,ini}$ and $\mathbf{q}_{m,fin}$ its initial and final small nodes, respectively. It is well known that if the function ψ_h belongs to the space of nodal Lagrangian finite elements of degree $r+1$, then $\operatorname{grad}\psi_h$ belongs to the first family of Nédélec finite elements of degree $r+1$, and clearly $\int_{\mathbf{e}_m} \operatorname{grad}\psi_h = \psi_h(\mathbf{q}_{m,fin}) - \psi_h(\mathbf{q}_{m,ini})$. Therefore when using these canonical bases, the matrix that gives the circulations along the active small edges of the gradient of a nodal finite element function (knowing the values of this function at the nodes of the principal lattices in each mesh element) is the transposed of the all-node incidence matrix of the graph $\mathcal{G}_{ho}$.

Its geometrical realization in a tetrahedron is shown (in a fragmented version for a friendly visualization) in Figure 4. It is worthwhile to mention that the set of *active weights* is proved to be unisolvent in [22]. The structure shown in the Figure 4 has to be replicated on each tetrahedron $t \in T$. We thus obtain the high-order graph, $\mathcal{G}_{ho}$, over which we can construct the high-order spanning tree, $\mathcal{S}_{ho}$.

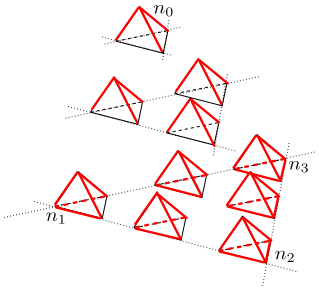

FIGURE 4 (Taken from reference [25]). A fragmented visualization of the geometrical realization of the connected graph in a tetrahedron with the active small edges (in red) as arcs and active small vertices as nodes.

4 | ALGORITHM FOR THE CONSTRUCTION OF THE SPANNING TREE (THE HIGH-ORDER CASE)

Thanks to the additional information given by the geometrical localization of the connected graph $\mathcal{G}_{ho}$, formed by the active small vertices and the active small edges (shown in Figure 4), we propose in the Algorithm 2 a suitable set of rules to construct a spanning tree in the referred graph $\mathcal{G}_{ho}$ for each tetrahedron; then we use this set of rules to construct a convenient *global* spanning tree $\mathcal{S}_{ho}$, giving in this way a classification rule in the set of active small edges of the mesh $\mathcal{T}$. The Algorithm 1 starts by reading the arcs of the spanning tree $\mathcal{S}$. We recall that, in a topologically trivial domain Ω, a spanning tree $\mathcal{S}$ can be obtained by applying algorithms such as the *Breadth-First search* or *Depth-First search* in the connected and directed graph $\mathcal{G}= (V, E)$. The arcs of $\mathcal{G}$ that are not in the spanning tree compose the cotree $\mathcal{S}^c$. For domains with no trivial topology, Algorithm 1 has to start from the arcs of a *belted-spanning-tree* $\mathcal{S}^b$, that can be obtained by applying Algortihm 3.

In Algorithm 1 the information on $\mathcal{S}$ is saved by mean of a flag associated with each edge of the mesh (if an edge is part of the spanning tree $\mathcal{S}$, the flag is set to `true`, otherwise is set to `false`); when the algorithm is initialized, the flag associated with each face is also set to `false` (we use this flag to control the previously visited face in the loop over all elements of the mesh).

The information saved in the flags is used within a loop over all the tetrahedra of the mesh, where the spanning tree $\mathcal{S}_{ho}$ is constructed; in each cycle of the tetrahedra loop, the previously proposed set of rules is used conveniently. The spanning tree $\mathcal{S}$ gives a selection criteria to put some active small edges of the global graph in the spanning tree $\mathcal{S}_{ho}$. More precisely, all the small edges on arcs of the spanning tree $\mathcal{S}$ and all but one (in particular the last one) the small edges on arcs of the cotree $\mathcal{S}^c$. Then the global spanning tree $\mathcal{S}_{ho}$ is further enriched with some active small edges at the interior of each face (only those faces of the tetrahedra that have not been visited previously), and finally with some active small edges

Algorithm 1 Initialization

Require: The mesh $\mathcal{T} = (V, E, F, T)$, and the first Betti number $g \geq 0$ of Ω.

Ensure: Logical tree-flag, visited-edge-flag and visited-face-flag arrays.

if $g == 0$ **then**
  Construct a spanning tree $\mathcal{S}^*$ of the graph (V, E) by using a Breadth-First search.
  Set $\mathcal{S} = \mathcal{S}^*$. ▷ If Ω is simply connected
else
  Construct a belted-spanning-tree $\mathcal{S}^b$ of the graph (V, E) by using Algorithm 3. ▷ If Ω is not simply connected
  Set $\mathcal{S} = \mathcal{S}^b$.
end if
loop over the edges $e \in E$
  tree-flag$(e) \leftarrow$ **false**.
  visited-edge-flag$(e) \leftarrow$ **false**.
  if $e \in \mathcal{S}$ **then**
    tree-flag$(e) \leftarrow$ **true**. ▷ Reading the spanning tree $\mathcal{S}$
  end if
end loop
loop over the faces $f \in F$
  visited-face-flag$(f) \leftarrow$ **false**.
end loop

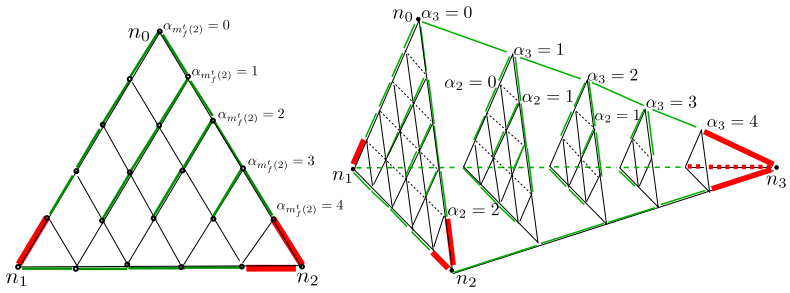

FIGURE 5 The spanning tree $\mathcal{S}_{ho}$ (in green) on a tetrahedron $t = [n_0, n_1, n_2, n_3]$. On the left, the subgraph corresponding to active small edges on the edges and in the interior of the face $f = [n_0, n_1, n_2]$, and the corresponding part of the spanning tree $\mathcal{S}_{ho}$. The red arcs belong to the spanning tree $\mathcal{S}_{ho}$, if and only if, its corresponding edge e belongs to the spanning tree $\mathcal{S}$. On the right, the active small edges in the interior of t belonging to $\mathcal{S}_{ho}$ are visualized, (note that for a friendly visualization, some active small edges were omitted in the figure). In this example we are considering $r = 4$.

at the interior of each tetrahedron. The proposed algorithm can be executed as part of pre-processing step. The algorithm requires as input the mesh $\mathcal{T}$ and the first Betti number g of the domain Ω; it gives as output the previously mentioned flags.

At a first sight, the Algorithm 2 seems to work on a graph $\mathcal{G}_{ho}$ with much more nodes and arcs than $\mathcal{G}$ (the one in the low-order case). In reality the high-order graph $\mathcal{G}_{ho}$ (and its incidence matrix) is not realized. We have used it only for visualization purposes. However, each arc in the high-order graph $\mathcal{G}_{ho}$ corresponds with a dof (and hence with an element of the canonical basis). Therefore any action on the set of dofs can be "visualized" as an action on this fictive graph. In Algorithm 2 we use only the low-order graph and make a local choice of dofs, this is done once on a reference element (as in Figure 5) and then applied repeatedly on the elements of the mesh. The local choice has to guarantee that the merge of all local spanning trees is a spanning tree of the (virtual) high-order graph, as illustrated in Figure 6. Algorithm 2 implements the choice illustrated in the figures.

In Figure 5 we can see the structure of the spanning tree $\mathcal{S}_{ho}$ (in green) given by the Algorithm 2, considering the case $r = 4$ in a mesh with a unique tetrahedron $t = [n_0, n_1, n_2, n_3]$; a red arc is in $\mathcal{S}_{ho}$ if its respective (big) edge is in the spanning tree $\mathcal{S}$, otherwise is out of $\mathcal{S}_{ho}$.

In Figure 6 we can see the structure of the spanning tree $\mathcal{S}_{ho}$ (in green and red) given by the Algorithm 2, considering the case $r = 4$ in a mesh with two tetrahedra. It is worth noting that the red arcs in this figure correspond to the red arcs in Figure 5 belonging to $\mathcal{S}_{ho}$.

Algorithm 2 A spanning tree of active small edges

Require: The mesh $\mathcal{T} = (V, E, F, T)$ and logical tree-flag, visited-edge-flag and visited-face-flag arrays.

Ensure: A (belted-) spanning tree $\mathcal{S}_{ho}$ of the graph $\mathcal{G}_{ho}$ with nodes: the active small vertices; and arcs: the active small edges.

loop over the tetrahedra $t \leftarrow [n_a, n_b, n_c, n_d] \in T$
  loop over the faces $f \leftarrow [n_i, n_j, n_k] \in \Delta_2(t)$
    if visited-face-flag(f) == **false then**
      loop over the edges $e \leftarrow [n_p, n_q] \in \Delta_1(f)$
        if visited-edge-flag(e) == **false then**
          if tree-flag(e) == **true then**
            add to $\mathcal{S}_{ho}$ the small edges $\{\boldsymbol{\alpha}, e\}$, $\forall\, \boldsymbol{\alpha} \in \mathcal{I}(4, r)$ with $\alpha_{m^t_{t-e}}(0) = 0$ and $\alpha_{m^t_{t-e}}(1) = 0$.
            ▷ All the small edges $\{\boldsymbol{\alpha}, e\}$ over the edge e.
          else
            add to $\mathcal{S}_{ho}$ the small edges $\{\boldsymbol{\alpha}, e\}$ for the $r-1$ *first* indices $\boldsymbol{\alpha} \in \mathcal{I}(4, r)$ with $\alpha_{m^t_{t-e}}(0) = 0$ and $\alpha_{m^t_{t-e}}(1) = 0$.
            ▷ *first* is always intended in the reversed lexicographical order.
          end if
          visited-edge-flag$(e) \leftarrow$ **true**
        end if
      end loop
      for $\alpha_{m^t_f(2)} \leftarrow 1$ **to** $r-1$ **do**
        add to $\mathcal{S}_{ho}$ the small edges $\{\boldsymbol{\alpha}, [n_{m_f(0)}, n_{m_f(1)}]\}$ for the $r - \alpha_{m^t_f(2)}$ *first* indices $\boldsymbol{\alpha} \in \mathcal{I}(4, r)$ with $\alpha_{m^t_{t-f}}(0) = 0$.
        ▷ Adding small edges $\{\boldsymbol{\alpha}, [n_{m_f(0)}, n_{m_f(1)}]\}$ of the interior of f to $\mathcal{S}_{ho}$.
      end for
      visited-edge-flag$(f) \leftarrow$ **true**
    end if
  end loop
  for $\alpha_3 \leftarrow 1$ **to** $r-2$ **do**
    for $\alpha_2 \leftarrow 1$ **to** $r - (\alpha_3 + 1)$ **do**
      add to $\mathcal{S}_{ho}$ the small edges $\{\boldsymbol{\alpha}, [n_{m_f(0)}, n_{m_f(1)}]\}$ for the $r - (\alpha_2 + \alpha_3)$ *first* indices $\boldsymbol{\alpha} \in \mathcal{I}(4, r)$.
      ▷ Adding small edges $\{\boldsymbol{\alpha}, [n_{m_t(0)}, n_{m_t(1)}]\}$ of the interior of t to $\mathcal{S}_{ho}$.
    end for
  end for
end loop

Proposition 2. If Ω is simply connected, the number $d_{S_{ho}}$ of small edges in $\mathcal{S}_{ho}$ is $(d_L - 1)$.

Proof. For $r = 0$, the small edges coincide with the mesh edges and their number in $\mathcal{S}$ is $(N_V - 1)$. Moreover, $N_V = d_L$, thus the property holds true for $r = 0$.

For $r > 0$, we recall that d_L can be rewritten as

$$d_L = N_V + N_E \dim \mathcal{P}_{r-1}(e) + N_F \dim \mathcal{P}_{r-2}(f) + N_T \dim \mathcal{P}_{r-3}(t)$$

where N_V (resp., N_E, N_F, N_T) is the number of nodes (resp., edges e, faces f, tetrahedra t) in the mesh over $\bar{\Omega}$. By the proposed algorithm, the number $d_{S_{ho}}$ of active small edges in the spanning tree $\mathcal{S}_{ho}$ can be counted as follows

$$d_{S_{ho}} = (r+1)\,\#\mathcal{S} + r\,\#\mathcal{S}^c + N_F \sum_{q=1}^{r-1}(r-q) + N_T \sum_{q=1}^{r-2}\Big[\sum_{s=1}^{r-(q+1)} r - (q+s)\Big]$$

with cardinalities $\#\mathcal{S} = (N_V - 1)$ and $\#\mathcal{S}^c = N_E - (N_V - 1)$. Note that

$$\sum_{q=1}^{r-1}(r-q) = r\sum_{q=1}^{r-1} 1 - \sum_{q=1}^{r-1} q = r(r-1) - \frac{r(r-1)}{2} = \frac{r(r-1)}{2} = \dim \mathcal{P}_{r-2}(f).$$

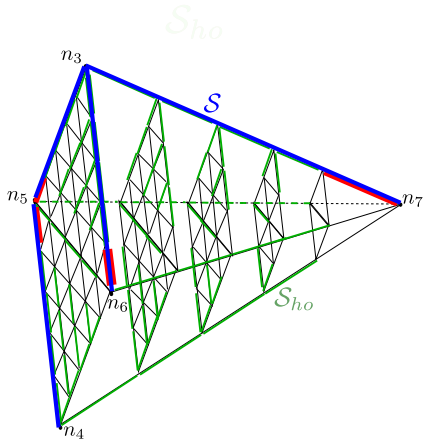

FIGURE 6 The spanning tree $\mathcal{S}_{ho}$ (in green and red) on a mesh $\mathcal{T}$ with two tetrahedra. The arcs of the spanning tree $\mathcal{S}$ in blue. It is worth noting that the red arcs in this figure correspond to the red arcs in Figure 5 belonging to $\mathcal{S}_{ho}$. In this example we are considering $r = 4$.

Moreover, for the last term in $d_{S_{ho}}$ we have

$$\begin{aligned}
&\sum_{q=1}^{r-2}[\sum_{s=1}^{r-q-1}(r-q-s)] = \sum_{q=1}^{r-2}[(r-q)\sum_{s=1}^{r-q-1}1 - \sum_{s=1}^{r-q-1}s] \\
&= \frac{1}{2}\sum_{q=1}^{r-2}[(r-q)(r-q-1)] = \frac{1}{2}[\sum_{q=1}^{r-2}q^2 - (2r-1)\sum_{q=1}^{r-2}q + r(r-1)\sum_{q=1}^{r-2}1] \\
&= \frac{1}{2}[\frac{1}{6}(r-2)(r-1)(2r-3) - \frac{1}{2}(2r-1)(r-1)(r-2) + r(r-1)(r-2)] \\
&= \frac{1}{2}(r-1)(r-2)[\frac{r}{3} - \frac{1}{2} + \frac{1}{2} - r + r] = \frac{1}{6}r(r-1)(r-2)
\end{aligned}$$

that is indeed $\dim \mathcal{P}_{r-3}(t)$. Summing up, we get

$$d_{S_{ho}} = N_V - 1 + N_E \dim \mathcal{P}_{r-1}(e) + N_F \dim \mathcal{P}_{r-2}(f) + N_T \dim \mathcal{P}_{r-3}(t) = d_L - 1,$$

thus the property. □

Remark: If Ω is not simply connected, let g be the first Betti number of Ω, namely, the number of homologically independent non bounding cycles in Ω. The algorithm can be easily generalized to this case by replacing the global spanning tree, $\mathcal{S}$, with a global belted-spanning-tree [27,4], $\mathcal{S}^b$ that has g additional arcs. Hence, the number of arc in the high-order belted-spanning-tree $\mathcal{S}^b_{ho}$ is $d_{S^b_{ho}} = d_L - 1 + g$. For more details on the computation of g and the construction of a belted-spanning-tree, see [28,29,30,31,32]. Note that Algorithm 2 has to start from the logical arrays tree-flag, visited-edge-flag and visited-face-flag filled in considering the belted-spanning-tree $\mathcal{S}^b$. The latter can be constructed as detailed in Algorithm 3. For example, if Ω is an empty torus, we have $g = 2$ and a belted-spanning-tree is presented in Fig. 7 (right).

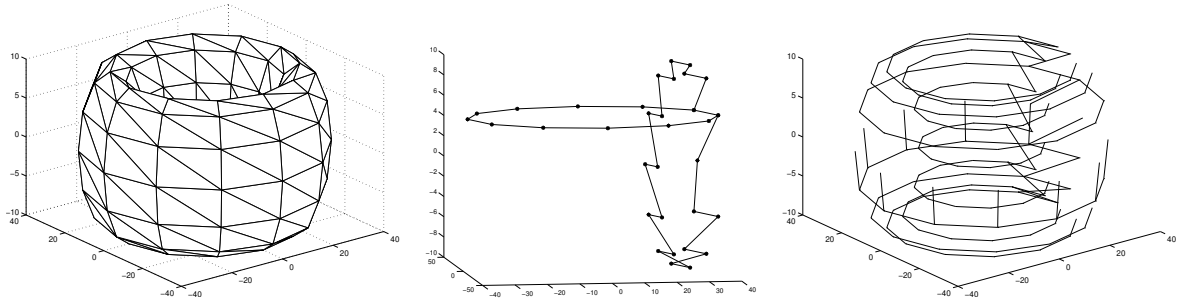

FIGURE 7 The mesh (left), the 2 cycles (center) and the belted-spanning-tree (right) computed from Algorithm 3.

Algorithm 3 Computing a belted-spanning-tree when Ω is not simply connected ($g > 0$)

Require: The mesh $\mathcal{T} = (V, E, F, T)$.
Ensure: A belted-spanning-tree $\mathcal{S}^b$.

Compute the g homologically independent not bounding cycles $\gamma_1, \gamma_2, ..., \gamma_g$ in $\mathcal{T}$.
▷ We assume that the g cycles $\gamma_1, \gamma_2, ..., \gamma_g$ are mutually disjoint and without self-intersection.
▷ This can be done by relying on the Smith normal form in $\mathbb{Z}$ as explained in [29,32].
for $i \leftarrow 1$ **to** g **do**
    consider the i-th disjoint cycle $\gamma_i = \sum_{e \in E} c_e^i \, e$, with $c_e^i \in \{-1, 0, 1\}$
    select one edge, say $e^i \in \gamma_i$, that does not belong to $\bigcup_{1 \leq j \leq i-1} \gamma_j$
    define $\tilde{\gamma}_i = \gamma_i \setminus \{e^i\}$
end for
    complete the acyclic sub-graph corresponding to $\bigcup_{i=1}^{g} \tilde{\gamma}_i$ to get a spanning tree $\mathcal{S}$ of the graph (V, E)
    define the belted-spanning-tree $\mathcal{S}^b = \mathcal{S} \bigcup_{i=1}^{g} \{e^i\}$.

It has to be said that in the lowest order case, the conditioning of the linear system gets worse once the gauge is applied and some work has been done to try to avoid it [33]. For the high-order case, some tests on three-dimensional eddy current problems are done in [34] where the magnetic vector potential based formulation is gauged by regularization instead of by the imposition of dofs associated with the arcs of a (belted) spanning tree. Some numerical tests will be done to see how badly the fact of gauging affects the "effective conditioning" of the system matrix in the high-order case, where effective conditioning means the ratio of eigenvalues of the matrix but not considering the (nearly) zero ones.

5 | CONCLUSIONS

The weights, namely integrals over mesh sub-simplices, are natural dofs to adopt when the solution is a cochain on a simplicial mesh. They allow to extend straightforwardly the classical tree-cotree techniques from the low-order to the high-order case, since there is a correspondence of dofs with geometrical entities, the small simplices, that constitute a graph. In this work we have presented an algorithm for the construction of a (belted) spanning tree of this graph. The construction is based on a (belted) spanning tree of the graph given by vertices and edges of the mesh (the so-called global (belted) spanning tree). Then a loop by elements enriches this initial (belted) spanning tree with arcs corresponding to face dofs (only those faces of the tetrahedra that have not been visited previously) and with the arcs corresponding to the volume dofs. The enrichment in each element is the same for all elements. Gauging through such a tree-cotree approach (applied to the dual graph with the small triangles as vertices and the small edges in common as arcs) has been successfully applied in the frame of high-order reconstructions of a Darcy flow in a 2D domain starting from its weights on the small edges [35]. Further numerical investigations are however necessary to analyze how this gauging influences the conditioning of the final algebraic system associated with an electromagnetic problem.

ACKNOWLEDGMENTS

Financial disclosure

Financial support from the French MathIT program ANR-15-IDEX-01 and the Italian project PRIN 201752HKH8.

Conflict of interest

The authors declare no potential conflict of interests.

References

1. Bossavit A. Generating Whitney forms of polynomial degree one and higher. *IEEE Transactions on Magnetics* 2002; 38(2): 341-344. doi: 10.1109/20.996092

2. Rapetti F, Bossavit A. Geometrical localisation of the degrees of freedom for Whitney elements of higher order. *IET Science, Measurement & Technology* 2007; 1(1): 63–66.

3. Rapetti F, Bossavit A. Whitney forms of higher degree. *SIAM J. Numer. Anal.* 2009; 47(3): 2369–2386. doi: 10.1137/070705489

4. Kettunen L, Forsman K, Bossavit A. Formulation of the eddy current problem in multiply connected regions in terms of h. *Int. J. Numer. Methods Engrg.* 1998; 41: 935–954.

5. Bossavit A. *Computational Electromagnetism*. San Diego: Academic Press Inc. . 1998.

6. Bossavit A. Whitney forms: A class of finite elements for three-dimensional computations in electromagnetism. *IEE Proceedings A (Physical Science, Measurement and Instrumentation, Management and Education, Reviews)* 1988; 135(8): 493–500.

7. Nédélec JC. Mixed finite elements in $\mathbf{R}^3$. *Numer. Math.* 1980; 35: 315–341.

8. Barton M, Cendes Z. New vector finite elements for three-dimensional magnetic field computation. *Journal of Applied Physics* 1987; 61(8): 3919–3921.

9. Albanese R, Rubinacci G. Integral formulation for 3D eddy-current computation using edge elements. *IEE Proceedings A (Physical Science, Measurement and Instrumentation, Management and Education, Reviews)* 1988; 135(7): 457–462.

10. Albanese R, Rubinacci G. Magnetostatic field computations in terms of two-component vector potentials. *Int. J. Numer. Meth. Engnrg.* 1990; 29: 515–532.

11. Manges JB, Cendes ZJ. A generalized tree-cotree gauge for magnetic field computation. *IEEE Transactions on Magnetics* 1995; 31(3): 1342–1347.

12. Webb J, Forghani B. A single scalar potential method for 3D magnetostatics using edge elements. *IEEE Transactions on Magnetics* 1989; 25(5): 4126–4128.

13. Albanese R, Coccorese E, Martone R, Miano G, Rubinacci G. On the numerical solution of the nonlinear three-dimensional eddy current problem. *IEEE transactions on magnetics* 1991; 27(5): 3990–3995.

14. Nédélec JC. Mixed finite elements in $\mathbf{R}^3$. *Numer. Math.* 1980; 35(3): 315–341. doi: 10.1007/BF01396415

15. Nédélec JC. A new family of mixed finite elements in $\mathbf{R}^3$. *Numer. Math.* 1986; 50(1): 57–81. doi: 10.1007/BF01389668

16. Monk P. *Finite element methods for Maxwell's equations*. Numerical Mathematics and Scientific ComputationOxford University Press, New York . 2003

17. Rapetti F. Comments on a High-Order Whitney Complex for Simplices. *IEEE Journal on Multiscale and Multiphysics Computational Techniques* 2019; 4: 348–355.

18. Rapetti F. High order edge elements on simplicial meshes. *M2AN Math. Model. Numer. Anal.* 2007; 41(6): 1001–1020. doi: 10.1051/m2an:2007049

19. Rapetti F. Weights computation for simplicial Whitney forms of degree one. *C. R. Math. Acad. Sci. Paris* 2005; 341(8): 519–523. doi: 10.1016/j.crma.2005.09.005

20. Alonso Rodríguez A, Rapetti F. Some remarks on spanning families and weights for high order Whitney spaces on simplices. *Comput. Math. Appl.* 2019; 78(9): 2961–2972. doi: 10.1016/j.camwa.2019.03.006

21. Alonso Rodríguez A, Rapetti F. The discrete relations between fields and potentials with high order Whitney forms. In: . 126 of *Lect. Notes Comput. Sci. Eng.* Springer, Cham. 2019 (pp. 259–267)

22. Alonso Rodríguez A, Bruni Bruno L, Rapetti F. Minimal sets of unisolvent weights for high order Whitney forms on simplices. In: Lect. Notes Comput. Sci. Eng. Springer, Cham. 2020 (pp. 195–203).

23. Rapetti F, Alonso Rodríguez A. High Order Whitney Forms on Simplices and the Question of Potentials. In: Lect. Notes Comput. Sci. Eng. Springer, Cham. 2020 (pp. 1–16).

24. Arnold DN, Falk RS, Winther R. Finite element exterior calculus, homological techniques, and applications. *Acta Numer.* 2006; 15: 1–155. doi: 10.1017/S0962492906210018

25. Christiansen S, Rapetti F. On high order finite element spaces of differential forms. *Mathematics of Computation* 2016; 85(298): 517–548.

26. Arnold DN, Falk RS, Winther R. Geometric decompositions and local bases for spaces of finite element differential forms. *Computer Methods in Applied Mechanics and Engineering* 2009; 198(21-26): 1660-1672.

27. Kettunen L, Forsman K, Bossavit A. Discrete spaces for div and curl-free fields. *IEEE Trans. Magn.* 1998; 34: 2551–2554.

28. Hiptmair R, Ostrowski J. Generators of $H_1(\Gamma_h, \mathbb{Z})$ for triangulated surfaces: construction and classification. *SIAM J. Comput.* 2002; 31(5): 1405–1423. doi: 10.1137/S0097539701386526

29. Rapetti F, Dubois F, Bossavit A. Discrete vector potentials for non-simply connected three-dimensional domains. *SIAM J. on Numerical Analysis* 2003; 41: 1505-1527.

30. Dlotko P, Specogna R, Trevisan F. Automatic generation of cuts on large-sized meshes for the $T - \Omega$ geometric eddy-current formulation. *Computer Methods in Applied Mechanics and Engineering* 2009; 198: 3765-3781.

31. Alonso Rodríguez A, Bertolazzi E, Ghiloni R, Valli A. Construction of a finite element basis of the first de Rham cohomology group and numerical solution of 3D magnetostatic problems. *SIAM J. Numer. Anal.* 2013; 51(4): 2380–2402. doi: 10.1137/120890648

32. Pellikka M, Suuriniemi S, Kettunen L, Geuzaine C. Homology and cohomology computation in finite element modeling. *SIAM Journal on Scientific Computing* 2013; 35(5): B1195–B1214.

33. Ren Z, Razek A. Boundary edge elements and spanning tree technique in three-dimensional electromagnetic field computation. *Int. J. Numer. Methods Engrg.* 1993; 36: 2877–2893.

34. Ledger PD, Zaglmayr S. hp-Finite element simulation of three-dimensional eddy current problems on multiply connected domains. *Comp. Meth. Appl. Mech. Engng.* 2010; 199(49-52): 3386–3401.

35. Alonso Rodríguez A, Rapetti F, Zappon E. New degrees of freedom for high-order Whitney approximations of Darcy's flows. *Num. Alg.* 2020; 87: 1613-1634.

How to cite this article: E. De Los Santos, A. Alonso Rodríguez, and F. Rapetti (2022), Construction of a spanning tree for high-order edge elements